2024 IEEE International Conference on Robotics and Automation (ICRA 2024)
May 13-17, 2024. Yokohama, Japan

# Environment-Modulated Self-Assembly by Changes in Modules' Buoyancy

Xiao Chen[1], Junyi Han[1], Xin Jin[1] and Shuhei Miyashita[1,2]

***Abstract*— While many inkjet printers employ only four types of ink (i.e. CKMY) to produce a wide range of colors, numerous technical challenges still exist for contemporary 3D printers to fabricate various materials and generate composite products such as electric devices. Conversely, there have been attempts and endeavors to make things through self-assembly of parts, analogous to the autonomous and decentralized development process of the human body from just 20 types of amino acids. In our previous work, we proposed a method for the rapid production of 3D objects using the centimeter-sized modules (referred to as Roblets) capable of generating a 2D structure and subsequently self-folding themselves into a 3D configuration, akin to origami. To further leverage the capability of generating a wide variety of different types of structures by combining different modules, this research studies a method of automatically selecting and supplying modules using environmental cues. More precisely, we developed a mechanism to couple different modules corresponding to three different environments (on a flat surface, on low-dense saline, and on saturated saline) and yielded different module configurations. The process of self-assembly necessitated the application of perturbation, which was realized by imparting magnetic torque originating from an external magnetic field onto the magnets embedded in the modules.**

## I. Introduction

The manufacturing technology of building things bottom-up, mimicking the ability of living organisms, has remained a major challenge in engineering. Likewise, amino acids synthesize into proteins in decentralized ways, establishing a manufacturing technology whereby components interact with each other and spontaneously self-assemble into a three-dimensional structure would not only enable hands-free production of a wide variety of things but also realize resilient structures. It could also advance the manufacturing technology at the microscale.

A series of molecular scale DNA self-assembly studies have revealed that a certain condition enables self-assembling systems: The continuous repetition of module collisions over and over again so that only connections that happen to be matched can retain their bonds and eventually leading to the parallel formation of the final shapes (so-called "Proofreading by massive sampling"). Many studies on self-assembly at the millimeter- and centimeter-scales have been conducted with the aim of reproducing all or part of this condition: e.g. components interacting with each other by the built-in magnets [1], [2], [3], [4], [5], [6], capillary force [7], [8], or gravitation [9], being mechanically perturbed [6], [10], [11], [12], magnetically perturbed [13], [14], [15], or self-propulsive [16], [17].

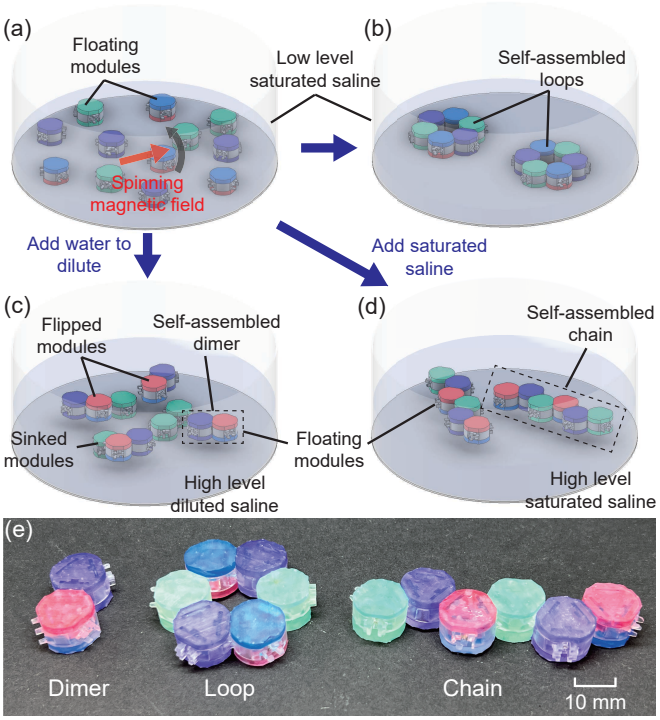


Fig. 1. The proposed self-assembly method produces different configurations of clusters. The shape of the clusters created differs when mechanical perturbations are applied from a random arrangement of modules (a→b), or when water is added, some modules sink, and some modules are inverted into their vertical positions (a→c). Or, different liquid affects assembly results (a→d). Perturbation can be managed by applying a magnetic field. (b) Two loop configurations self-assembled on a low-level saturated saline. (c) Four dimer configurations self-assembled on high-level diluted saline. (d) Two chain configurations self-assembled on high-level saturated saline. (e) The photo of different configurations: dimer that consists of two modules, loop, and chain.

As artificial self-assembly of components is generally a long time-consuming process or with not high completion rates, an alternative method has been investigated in recent years inspired by the origami folding technique, which aims to generate a 3D structure by folding a 2D plane [18], [19], [20]. The origami-inspired approach has shown some success but a problem has remained on the transformability that a new self-folding sheet has to be produced for each different shape, and although the method is effective in the rapid construction of things, there has been room for improvement as a manufacturing tool.

To address this problem, in our previous study [21], we presented *Roblets*, self-assembling modules that self-

[1]Automatic Control and Systems Engineering Department, University of Sheffield, Sheffield S1 3JD, UK. shuhei.miyashita@sheffield.ac.uk [2]Insigneo Institute for *in silico* Medicine.

assemble into a 2D pattern, then self-fold into a 3D shape. The 3D shape can then be actuated instantly as a robot by an operator using an external magnetic field, to perform simple tasks such as picking and placing an object whose size is larger than the individual modules. While the method has shown innovative performance as a means of more rapid prototyping, where the process begins with the assembly of components, it has yielded a need to realize an automatic component supply mechanism.

Referring to the above issues, this study enables a new way of selecting and supplying self-assembly components by actively modifying the environment. Specifically, by creating three different environments, where the components are either on a low-level water surface, floating on low-dense liquid (water or diluted saline), or floating on a high-dense liquid (saturated saline), and realizing a mechanism whereby particular components float, sink, and flip upside down under respective conditions and thereby bond to different components, different configurations of two-dimensional structures are self-assemblable. Fig. 1 shows an overview of the study, depicting the self-assembly of discrete components (Fig. 1 (a)) into a hexamer (loop structure) structure on a low-level saline surface (Fig. 1 (b)), into a dimer on a high-level diluted saline surface (Fig. 1 (c)), and into a chain on a high-level saturated saline surface (Fig. 1 (d)). The contributions of the study are:

1) The concept and implementation of self-assembly, where the generation of structures is modulated by environmental change.
2) Use of an external magnetic field for the self-assembly of centimeter-sized modules.
3) Model of the dynamics of the self-assembly process and its simulation.

## II. Methods

### A. Buoyancy change induced module supply

The mechanism of selecting and supplying self-assembly components is achieved by varying the density of the environment to select and deselect modules that are developed with different densities to be engaged in 2D self-assembly at a particular height plane. For the modules shown in Fig. 1, we designed three different parts: main body, shelled cap, and solid cap (Fig. 2 (a)). The main body holds three bonding sites, which are used to connect with other modules, and three disk neodymium magnets ($\varnothing 2\,\text{mm} \times 0.5\,\text{mm}$, N42 grade, First4Magnets) installed perpendicular to each bonding site, with a pole facing outward. The module parts were fabricated by a SLA 3D printer (Formlabs Form 2, clear resin, $\rho_{resin}$ = 1.15 g/cm$^3$).

The shelled cap and solid cap are used to adjust the center of gravity (COG) and the total average density of the module. The two parts are designed to have the same external volume to ensure the same buoyancy in the water. By adjusting the position of the two parts, different types of modules with different average densities and centers of gravity can be produced (Fig. 2 (b)), which are the floating module, sinkable

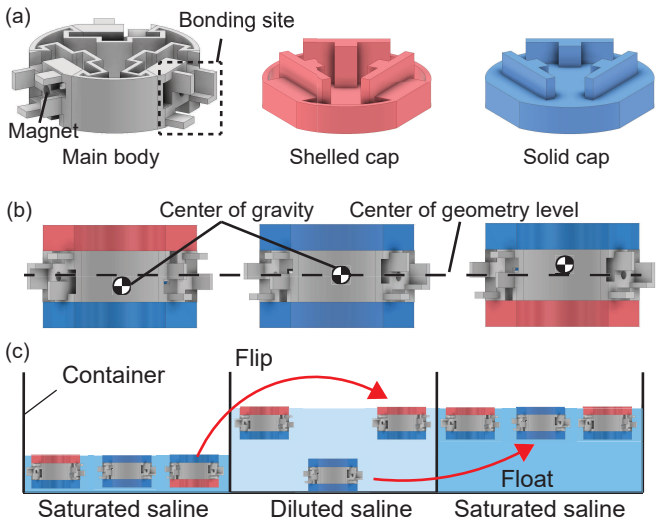


Fig. 2. Illustrations of different parts, module types, and modules state changing in different environments. (a) Three parts of a module (main body, shelled cap, and solid cap). (b) Illustration of the center of gravity of three types of modules: floating, sinkable, and flippable module. (c) Different states of three types of modules in low-level saturated saline, high-level diluted saline, and high-level saturated saline.

module, and flippable module. For example, by aligning the solid cap at the top and the shelled cap at the bottom, the center of gravity of the module is above its geometric center, therefore when the module is placed in water, the bottom tends to face up. With the assistance of a vertical magnetic field, which causes the instability of the upright posture of the module, resulting in the module flipping in water. On the contrary, by aligning the shelled cap at the top and the solid cap at the bottom, the center of gravity of the module is located below the geometric center, so the module will not flip over in water but keep its original attitude and float on water. The flippable module responds differently in different water level environments. When the water level is low, the module has contact with the ground thus the module is constrained with flipping. While in the high water level, the tilt of the module is not constrained, therefore the module is able to complete the flip under the magnetic field perturbation.

The center of gravity height of a module, $h_{COG}$, can be found by integrating the weight and weighted average of the center of gravity positions of each differential unit $dh$. As the module is rotationally symmetric, it has a uniform mass distribution in each differential unit. Therefore the $h_{COG}$ of the module can be described by the following equation:

$$h_{COG} = \frac{1}{M}\int V_h\,\bar{\rho}_h\,dh, \tag{1}$$

where $M$ is the total mass of a module (1.3 g for floating and flipping module and 1.7 g for sinking module), $\bar{\rho}_h$ is the average density of the module in a specific differential unit $dh$, and $V_h$ is the volume of the module in $dh$.

Modifying the size of the enclosed chambers in the shelled cap allows for adjustment of the module's overall weight. Consequently, modules with varying enclosed chamber sizes

can exhibit divergent average densities while maintaining a constant total volume. This allows different types of modules distinct responses within an environment. In this study, two different liquid environments are produced, which are the diluted saline ($\rho_{diluted\,saline}$ = 1.1 g/cm$^3$) and the saturated saline environment ($\rho_{saline}$ = 1.2 g/cm$^3$). For the sinking module, the average density is designed to be between the density of diluted saline and saturated saline, therefore it will sink in diluted saline and float in saturated saline to participate in the assembly process.

The orientation of the magnets is arranged so that they act as one equivalent magnet from a distance at the center of the module represented as the red arrow, where one of the magnets is opposite to the other two as shown in Fig. 3 (a). We define the N-type arrangement as the equivalent magnet that has the same direction as the one whose north pole faces outwards, and the S-type arrangement as the opposite.

Smart glue, the method of realizing specific bonds using different shapes and the attraction of magnets [21], is used to determine the shape of the assembled structure, where the distance between two bonded modules is regulated, allowing the modules to have stronger bonding strength when they correctly bonded and a weak bonding strength when they incorrectly bonded. Two different types of smart glue are used in the design: symmetrical and asymmetrical shown in Fig. 3 (b). When a module flips, the smart glue embedded in this module also flips and transforms into a new smart glue whose tabs and blanks are mirrored along the horizontal plane. For the symmetrical smart glue, the flipped pattern is the same as the original pattern, therefore it can remain the connection with the previous complementary smart glue. For the asymmetrical smart glue, the pattern after flipping is different from the original pattern, which leads to it not being able to connect the bonding site with the previous complementary smart glue.

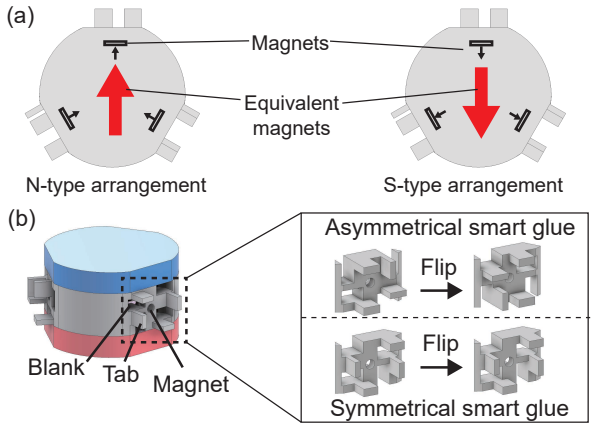


Fig. 3. Magnet arrangements and smart glue. (a) Two types of magnet arrangements: N-type arrangement, where the equivalent magnet has the same direction as the one whose north pole faces outwards, and S-type arrangement, where the equivalent magnet has the same direction as the one whose south pole faces outwards. (b) Two types of smart glue: asymmetrical and symmetrical smart glue.

### B. Magnetically induced self-assembly

The built-in magnets enable component-component interactions between modules, however, the self-assembly process also requires the assistance of environmental agitation, analogous to the thermal agitation of the molecular scale. In this study, an external magnetic field is used to directly perturb the self-assembly modules by means of magnetic torque, not inducing turbulence in the environment, but gradually changing the relative position between modules. As the magnetic field is applied, the built-in magnets tend to align with it, generating a magnetic torque. Given the three magnets in each module, the torque produced is equivalent to that of a single magnet, whose strength is the combined vector sum of the three individual magnets. The magnetic torque for the module can be derived using the following equation:

$$\tau_{module} = m_{module} B \sin\theta, \tag{2}$$

where $m_{module}$ is the equivalent magnetic moment of the module seen from a distance, and $\theta$ is the angle between the direction of the magnetic moment and the external magnetic field. When the magnetic field spins around an axis perpendicular to the workspace, the modules are prompted to spin, synchronizing with the direction of the field. Given the magnetic interactions between the modules, they are able to move freely across the water surface, attracting and occasionally colliding with one another.

The flux density and spinning speed of the magnetic field are regulated in two stages. The first stage is defined as the self-assembly stage, where the magnetic field spins at 1 rad/s with a flux density of 1 mT and lasts for 10 seconds, allowing modules to attract and bond with each other. The second stage is defined as the mismatch-correction stage, where the magnetic field accelerates to 40 rad/s with the flux density increasing to 3 mT and last for 3 seconds. The smart glue embedded in the modules allows them to bond at the correct position when they collide and shortens the distance between two modules, and provides a mechanical lock along the tangent line at the bonding point, making the modules spin as a single rigid body. Meanwhile, the smart glue also prevents the modules from forming a strong bond if the smart glue mismatches, and maintains a certain distance between the modules. This reduces the required torque to separate them [22].

### C. Chemical Kinetic Rate Model

The yield of the self-assembly process can be further modeled and simulated using the chemical kinetic rate model, where the total number of modules can exceed the limit of the experimental condition [1], [23], [24], [25]. In this study, we simulate the yield that multiple modules self-assemble into dimers, where the process is the foundation to construct a larger structure. Four different modules are designated and represented with state variables $X_A$, $X_B$, $X_C$, and $X_D$, where module $X_A$ and $X_B$ have a pair of complementary smart glue, allowing them to correctly bond as dimer $X_{ABcorrect}$. Similarly, module $X_C$ and $X_D$ can

correctly bond as dimer $X_{CDcorrent}$. The process of self-assembly of two modules into a dimer can be expressed by state transition equations, in which the two modules serve as reactants and the assembled dimer serves as the product, listed as follows:

$$\begin{array}{ll} \mathrm{X_A + X_A \rightleftharpoons X_{AA}}, & \mathrm{X_A + X_B \rightarrow X_{ABcorrect}}, \\ \mathrm{X_A + X_B \rightleftharpoons X_{ABincorrect}}, & \mathrm{X_A + X_C \rightleftharpoons X_{AC}}, \\ \mathrm{X_A + X_D \rightleftharpoons X_{AD}}, & \mathrm{X_B + X_C \rightleftharpoons X_{BC}}, \\ \mathrm{X_B + X_D \rightleftharpoons X_{BD}}, & \mathrm{X_C + X_D \rightarrow X_{CDcorrect}}. \\ \mathrm{X_C + X_D \rightleftharpoons X_{CDincorrect}}, & \mathrm{X_D + X_D \rightleftharpoons X_{DD}}, \end{array} \quad (3)$$

where the state transitions when forming correct bonded dimers ($X_{ABcorrect}$ and $X_{CDcorrect}$), which are considered non-detachable, are expressed as non-reversible state transitions, while other processes are reversible.

State vector $\vec{x} = (x_A, \ldots, x_{CD})$ is used to represent the number of each state variable $X_n$ ($n \in A, B, ..., DD$), denotes individual module or assembled dimer at every time step $t$, or more precisely, at every time that a collision happens. The time step can be mapped in seconds by multiplying the collision frequency. The state vector changes along the time step following the difference equation:

$$\vec{x}(t+1) = \vec{x}(t) + \vec{F}(x(t)), \quad (4)$$

where $\vec{F}$ is the variation of the number of $X_n$ at each time step, and it is determined with the equation:

$$F_n(x) = \sum_{i,j} \nu_{ij} P_{ij}^c P_{ij}^b + \sum_n \nu_n P_n^d x_n, \quad (5)$$

where $\nu_{ij}$ and $\nu_n$ represents stoichiometric numbers regarding the assembly and disassembly processes, $i$, $j$, $n \in \{A, B, ..., DD\}$ denote the type of modules or combination of dimers. $P_{ij}^c$ represents the collision probability between the modules, $P_{ij}^b$ represents the bonding probability when the collision happens between the modules, and $P_n^d$ represents the disassembly probability of a dimer. The collision probability $P_{ij}^c$ is assumed as the probability that randomly picks two modules $X_i$ and $X_j$ from all the individual modules and dimers, which can be simplified into the following equation:

$$P_{ij}^c = \begin{cases} 2x_i x_j / (\sum_n x_n)^2. & (i \neq j) \\ x_i^2 / (\sum_n x_n)^2. & (i = j) \end{cases} \quad (6)$$

The probability for two modules to bond upon collision depends on their attraction or repulsion, which is determined by the arrangement of the built-in magnets and the relative position of the modules, which is then simplified regarding the arrangement of the magnets in the modules. When two modules are synced with the spinning magnetic field, if they have different magnet arrangements (N-type and S-type), they tend to attract with each other at all times, however, only $2/3$ of time that two modules with the same magnet arrangements tend to attract. Regarding the magnet arrangements for the modules, where $X_A$, $X_C$, and $X_D$ have S-type arrangement, and $X_B$ have N-type arrangement, the bonding probability for two modules to correctly bond is experimentally derived as $1/6$. The disassembly is considered to occur only on the dimers where two modules are incorrectly bonded due to the weak bonding and mostly happens during the mismatch-correction stage. The disassembly probability is experimentally tested and derived as $0.1$ during the self-assembly stage, and $0.8$ during the mismatch-correction stage. Overall, with the time ratio of $10:3$ between the two stages, the disassembly probability $P^d$ can be further derived with a weighted average of $0.262$.

## III. Results

### A. Floating and flipping mechanism

Fig. 4 shows the flipping success rate of different modules with different COG in a deionized (DI) water environment ($\rho_{water}$ = 1.0 g/cm$^3$) and saturated saline environment. All the test modules were placed in the liquid with an upward center of gravity. As the overall weight distribution and average density of the modules were designed, the modules floated on water and the surface tension of the liquid stabilized the modules in their current attitude due to the large area of the module's bottom surface. With the induced variation of the external vertical magnetic field, modules can flip over because the center of gravity shift destroys the original surface tension, gravity and buoyancy balance.

As the vertical magnetic field increases, the module's tilt intensifies, increasing its probability of flipping. In addition, as the salinity increases, the submerged volume of the module decreases. The height of its COG with respect to the water surface is elevated, which reduces the stability of the module against perturbations and makes it more prone to flipping.

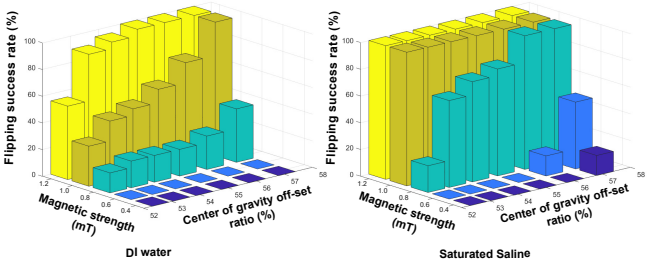


Fig. 4. Flipping success rate of different modules with the designed center of gravity in DI water, and saturated saline. Modules are perturbed by different strengths of a vertical magnetic field.

### B. Magnetic agitation

We first demonstrated the self-assembly process where two groups of modules with $8$ in total were involved, aimed to self-assemble into $4$ dimers perturbed by the spinning magnetic field. With the same condition used in the simulation, each group consisted of $4$ different modules ($X_A$, $X_B$, $X_C$, and $X_D$). Different magnet arrangements were applied on $X_A$ (N-type) and $X_B$ (S-type), and each of them had a complementary smart glue, that allowed them to bond into a dimer $X_{AB}$. Both $X_C$ and $X_D$ had the N-type magnet arrangements and were designed with a pair of complementary smart glue on each module, that allowed them to bond into a dimer $X_{CD}$. $X_A$ and $X_B$

cannot correctly bond with $X_C$ or $X_D$. The applied spinning magnetic field was controlled to periodically repeat the self-assembly and mismatch-correction stages.

Fig. 5 (a) shows the variation of the assembled modules through the experiment, where the x-axis represents the time and the y-axis represents the number of assembled modules. The values are obtained by visually sampling the video frames every 30 seconds. The blue line shows the number of all the bonded modules, including both correct and incorrect bonds. It shows that the modules rapidly bond together at the beginning, and separate incorrect bonds (shown as the wave) until all the modules correctly bond into dimers after 18 minutes and 20 seconds. The red line denotes only the correctly bonded modules which shows that all the correctly bonded dimers can retain their bonds till the end of the experiment. Fig. 5 (b) shows the self-assembly process in the first 2 minutes, where the blue line shows the variation of the number of all bonded modules that synchronized with the red line which denotes the spinning speed of the magnetic field. The values are obtained by visually sampling the video frames every 2 seconds. It shows that most of the disassembly, where incorrect bonds are separated, happens during the mismatch-correction stage where the magnetic field spins at a higher speed.

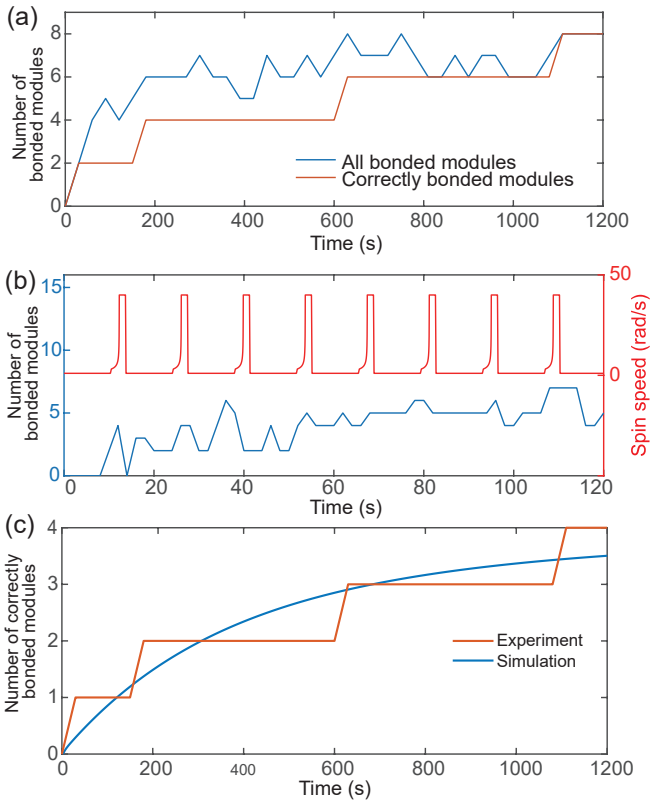


Fig. 5. Self-assembly and mismatch-correction regarding the spin speed of the magnetic field, and the simulation result of the chemical kinetic rate model (a) Number of modules that bonded over time, (b) Number of modules bonded regarding the spin speed of the magnetic field in the first 2 minutes, (c) Chemical kinetic rate model simulation result compare with the experimental result.

The simulation result of the kinetic rate model is shown in Fig. 5 (c), which shows the transition of the number of correctly bonded modules. The time step used in the simulation was mapped to real-time in seconds by multiplying the average collision frequency of 0.2667. It shows a similar trend that the self-assembly rapidly happens at the beginning, and ends up with all dimers correctly formed, which proves that the chemical kinetic rate model is eligible to simulate and predict the yield of the self-assembly process.

### C. Proof-of-concept demonstrations

Fig. 6 illustrates the three proof-of-concept demonstrations of environment-modulated self-assembly. 12 modules were randomly placed on the surface of a container with low water level (height = 8 mm) saturated saline. By applying an external time-varying magnetic field shown in Fig. 5 (b), the modules connected correctly after collisions and form two loop structures (Fig. 6 (a)). High water level diluted saline was added to the container (height = 22 mm). Modules with different average densities responded differently: modules with high average densities remain to sink in the bottom of the container; the rest modules floated on the water surface with different postures. With the external vertical magnetic field variation, some modules floated on water with their original gestures, and some modules float with a 180° inversion (flip). By applying the same spinning magnetic field, the flipped modules connected to the floating modules to assemble four dimer configurations (Fig. 6 (b)). With high water level saturated saline (height = 22 mm), the density of the water increased. The floating modules and flipping modules had the same situation compared with Fig. 6 (b). While the sinking modules started floating on the surface. By applying the same agitation, the sinking modules participated in the self-assembly process and constructed several chain configurations (Fig. 6 (c)). Modules took 19 minutes to form in loop configurations, 10 minutes to form in dimer configurations, and 10 minutes to form in chain configurations. Experiments were carried out in five trials for each environment. The average rate of correct bonding of different configurations is 68.3%, 91.7%, and 76%. The number of modules and assembled configuration design influence the assembly time and correcting bonding rate. With less number of modules involved in the process, fewer collisions occur, thus it requires more time for the modules to be correctly assembled. However, a large number of modules will accumulate into large clusters, thus the incorrect bonding rate will increase and the module have less space to adjust/alter the relative position.

## IV. Conclusion

This paper proposes the use of environmental alterations as a novel provisioning approach for self-assembling modules. By exploiting variations in module buoyancy across distinct environments, the self-assembly of three types of configurations was demonstrated. The agitation of the self-assembly process was achieved through the imposition of a magnetic field, and the kinetics were modeled and compared

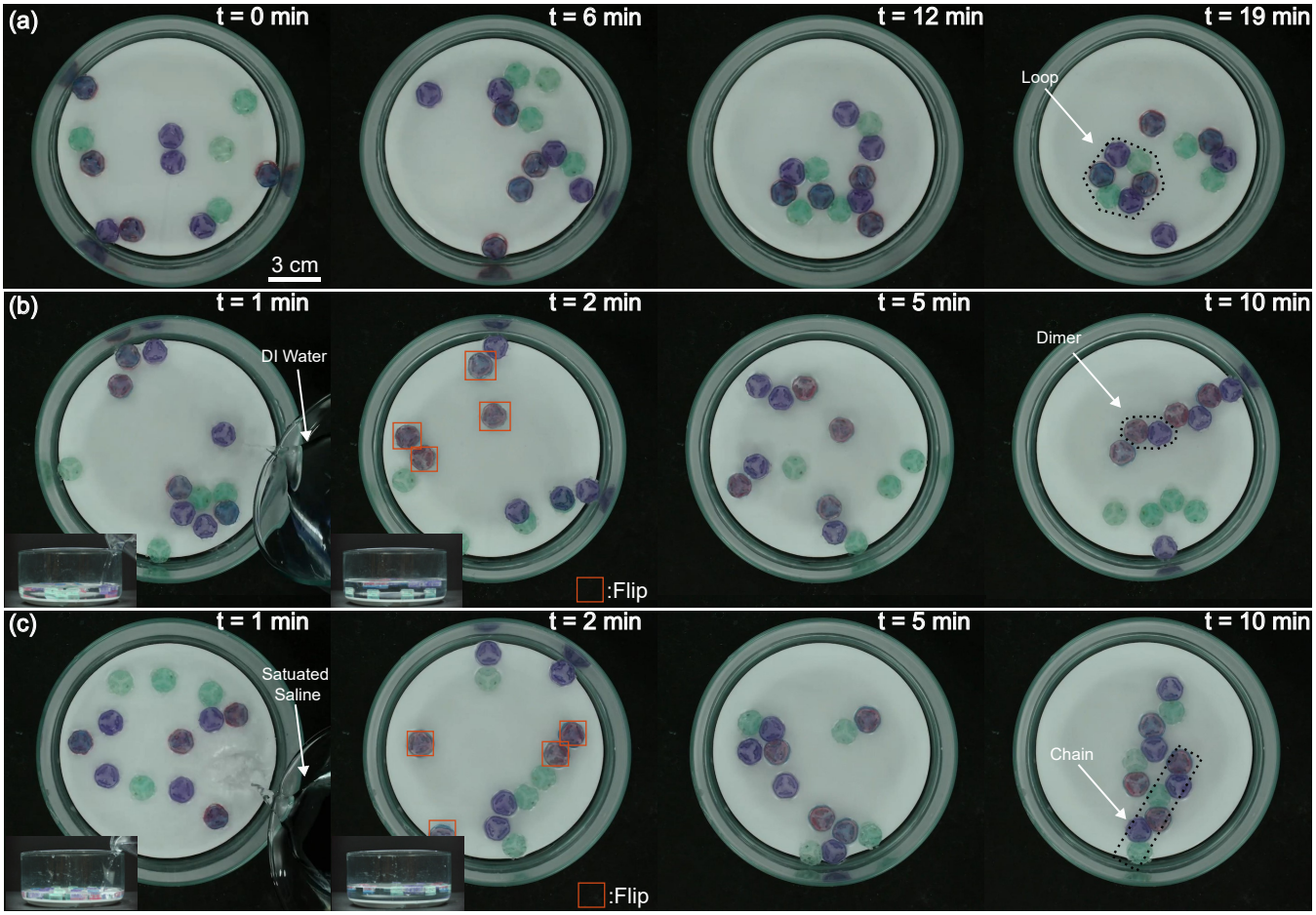


Fig. 6. Proof of concept demonstration throughout the three different environments; (a) Loop configurations in low water level saturated saline; (b) Dimer configurations in high water level diluted saline; (c) Two chain configurations in high water level saturated saline. All self-assembly processes were induced by the application of external magnetic field. See the supplemental video for more details.

with the experimental results. The obtained results support the environment-modulated self-assembly, which will open a new way of module supply in a self-assembly system.

## ACKNOWLEDGMENT

We thank Yuandong Guo and Takeru Katagiri for their support in conducting experiments, and other members of Sheffield Microrobotics Lab for assistance and feedback with the project.

## REFERENCES

[1] K. Hosokawa, I. Shimoyama, and H. Miura, "Dynamics of self-assembling systems: Analogy with chemical kinetics," *Artificial Life*, vol. 1, pp. 413–427, 1994.

[2] P. White, K. Kopanski, and H. Lipson, "Stochastic self-reconfigurable cellular robotics," in *IEEE International Conference on Robotics and Automation (ICRA)*, vol. 3, 2004, pp. 2888–2893.

[3] E. Klavins, "Programmable self-assembly," *IEEE Control Systems Magazine*, vol. 27, no. 4, pp. 43–56, 2007.

[4] D. Tsutsumi and S. Murata, "Multistate part for mesoscale self-assembly," in *SICE Annual Conference 2007*, 2007, pp. 890–895.

[5] N. Bhalla, P. J. Bentley, P. D. Vize, and C. Jacob, "Programming and evolving physical self-assembling systems in three dimensions," *Natural Computing*, vol. 11, pp. 475–498, 2012.

[6] A. Masumori and H. Tanaka, "Morphological computation on two dimensional self-assembly system," in *ACM SIGGRAPH 2013 Posters*, 2013, pp. 1–1.

[7] D. H. Gracias, J. Tien, T. L. Breen, C. Hsu, and G. M. Whitesides, "Forming electrical networks in three dimensions by self-assembly," *Science*, vol. 289, no. 5482, pp. 1170–1172, 2000.

[8] N. Bowden, S. R. Oliver, and G. M. Whitesides, "Mesoscale self-assembly: capillary bonds and negative menisci," *The Journal of Physical Chemistry B*, vol. 104, no. 12, pp. 2714–2724, 2000.

[9] R. Groß, S. Magnenat, and F. Mondada, "Segregation in swarms of mobile robots based on the brazil nut effect," in *2009 IEEE/RSJ International Conference on Intelligent Robots and Systems (IROS)*. IEEE, 2009, pp. 4349–4356.

[10] S. Miyashita, Z. Nagy, B. J. Nelson, and R. Pfeifer, "The influence of shape on parallel self-assembly," *Entropy*, vol. 11, no. 4, pp. 643–666, 2009.

[11] M. Matsumoto and S. Hashimoto, "Passive self-replication of millimeter-scale parts," *IEEE Transactions on Automation Science and Engineering (T-ASE)*, vol. 6, no. 2, pp. 385–391, 2009.

[12] B. Haghighat, E. Droz, and A. Martinoli, "Lily: A miniature floating robotic platform for programmable stochastic self-assembly," in *2015 IEEE International Conference on Robotics and Automation (ICRA)*, 2015, pp. 1941–1948.

[13] S. Miyashita, E. Diller, and M. Sitti, "Two-dimensional magnetic micro-module reconfigurations based on inter-modular interactions," *The International Journal of Robotics Research (IJRR)*, vol. 32, no. 5, pp. 591–613, 2013.

[14] E. Diller, N. Zhang, and M. Sitti, "Modular micro-robotic assembly through magnetic actuation and thermal bonding," *Journal of Micro-Bio Robotics*, vol. 8, no. 3-4, pp. 121–131, 2013.

[15] W. Wang, G. Gardi, P. Malgaretti, V. Kishore, L. Koens, D. Son, H. Gilbert, Z. Wu, P. Harwani, E. Lauga *et al.*, "Order and information in the patterns of spinning magnetic micro-disks at the air-water interface," *Science Advances*, vol. 8, no. 2, p. eabk0685, 2022.

[16] S. Miyashita, M. Kessler, and M. Lungarella, "How morphology affects self-assembly in a stochastic modular robot," in *2008 IEEE International Conference on Robotics and Automation (ICRA)*, 2008, pp. 3533–3538.

[17] M. J. Doyle, J. V. A. Marques, I. Vandermeulen, C. Parrott, Y. Gu, X. Xu, A. Kolling, and R. Groß, "Modular fluidic propulsion robots," *IEEE Transactions on Robotics*, vol. 37, no. 2, pp. 532–549, 2020.

[18] C. H. Belke and J. Paik, "Mori: a modular origami robot," *IEEE/ASME Transactions on Mechatronics*, vol. 22, no. 5, pp. 2153–2164, 2017.

[19] S. Miyashita, S. Guitron, S. Li, and D. Rus, "Robotic metamorphosis by origami exoskeletons," *Science Robotics*, vol. 2, no. 10, p. eaao4369, 2017.

[20] C. Sung, R. Lin, S. Miyashita, S. Yim, S. Kim, and D. Rus, "Self-folded soft robotic structures with controllable joints," in *2017 IEEE International Conference on Robotics and Automation (ICRA)*, 2017, pp. 580–587.

[21] J. Han, D. Rus, and S. Miyashita, "Roblets: Robotic tablets that self-assemble and self-fold into a robot," in *2023 IEEE/RSJ International Conference on Intelligent Robots and Systems (IROS)*. IEEE, 2023, pp. 4709–4714.

[22] M. Salehizadeh and E. Diller, "Two-agent formation control of magnetic microrobots in two dimensions," *Journal of Micro-Bio Robotics*, vol. 12, pp. 9–19, 2017.

[23] D. T. Gillespie, "Stochastic simulation of chemical kinetics," *Annu. Rev. Phys. Chem.*, vol. 58, pp. 35–55, 2007.

[24] L. Matthey, S. Berman, and V. Kumar, "Stochastic strategies for a swarm robotic assembly system," in *2009 IEEE International Conference on Robotics and Automation (ICRA)*, 2009, pp. 1953–1958.

[25] G. Mermoud, J. Brugger, and A. Martinoli, "Towards multi-level modeling of self-assembling intelligent micro-systems," in *Proceedings of the 8th International Conference on Autonomous Agents and Multiagent Systems (AAMAS)*, vol. 1, 2009, pp. 89–93.